AIP Applied Physics Letters

Efficient simulation of the impact of interface grading on the transport and optical properties of semiconductor heterostructures

X. Lü, L. Schrottke, E. Luna, and H. T. Grahn

Citation: Applied Physics Letters **104**, 232106 (2014); doi: 10.1063/1.4882653
View online: http://dx.doi.org/10.1063/1.4882653
View Table of Contents: http://scitation.aip.org/content/aip/journal/apl/104/23?ver=pdfcov
Published by the AIP Publishing

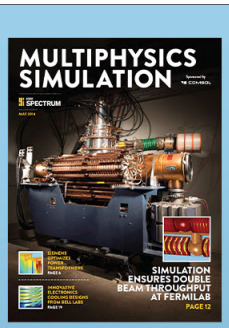

Efficient simulation of the impact of interface grading on the transport and optical properties of semiconductor heterostructures

X. Lü, L. Schrottke, E. Luna, and H. T. Grahn
Paul-Drude-Institut für Festkörperelektronik, Hausvogteiplatz 5–7, 10117 Berlin, Germany

(Received 27 March 2014; accepted 29 May 2014; published online 10 June 2014)

An efficient model is proposed to evaluate the impact of interface grading on the properties of semiconductor heterostructures. In the plane-wave approximation, the interface grading is taken into account by simply multiplying the Fourier components of the potential by a Gaussian function, which results only in a very small increase of the computation time. We show that the interface grading may affect the transition energies, the field strength for resonant coupling of subbands, and even the miniband formation in complex systems such as quantum-cascade lasers. This model provides a convenient tool for the incorporation of interface grading into the design of heterostructures. © *2014 AIP Publishing LLC*. [http://dx.doi.org/10.1063/1.4882653]

The simulation of the transport and optical properties of semiconductor heterostructures is of great interest for both, the understanding of physical processes and the performance improvement of optoelectronic devices. Heterostructures are layer sequences based on at least two materials with different energy gaps. The heterostructures may be simple quantum wells (QWs) or complex structures such as superlattices and quantum-cascade lasers (QCLs). The corresponding conduction and valence band edge profiles are well described by step-like functions of the potential at the heterointerface. For a better agreement with the experimental data, the nonparabolicity of the bulk band structure is often taken into account, and the resultant energy-dependent effective mass can be easily treated by applying a pseudo $\mathbf{k}\cdot\mathbf{p}$ model with at least two bands.

The growth of such layer sequences is affected by intermixing and island growth. Therefore, the profile at the interface is more adequately described by a gradual transition rather than an abrupt change of the materials composition, i.e., of the band profile. Calculations for GaAs/(Al,Ga)As and *p*-Si/SiGe QWs show that the interface broadening can result in a wavefunction distortion,[1] change of energy levels,[2] and dominant alloy disorder scattering.[3,4] Furthermore, interface scattering has an important impact on the transport and optical properties of GaAs QWs,[5] (In,Ga)As/(In,Al)As mid-infrared (MIR) QCLs,[6] (In,Ga)As/Ga(As,Sb) (Ref. 7) and GaAs/(Al,Ga)As THz QCLs.[8] In Ref. 1, the Al composition profile of GaAs/(Al,Ga)As QWs is modeled by an error function. The simulated Al profiles including anodic-oxide-induced interdiffusion are in agreement with those determined by transmission electron microscopy.[9] The interface may extend to 1.36 nm, i.e., 4.8 monolayers (MLs), where the thickness of one ML is 0.2825 nm. Furthermore, the formation of growth islands in GaAs/(Al,Ga)As single QWs can lead to disorder at the interfaces and obviously influence the excitonic lineshape and linewidth in corresponding photoluminescence spectra.[10,11] Therefore, interface grading may play an important role for the transport and optical properties of QW systems.

There are only a few studies of the interface grading effect on the properties of complex quantum structures such as GaAs/(Al,Ga)As QCLs. Roberts *et al.*[12] investigated GaAs/$Al_{0.45}Ga_{0.55}$As MIR QCLs assuming a linear profile for the compositional grading. Anders *et al.*[13] reported a shift of the emission wavelength for MIR GaAs/$Al_{0.4}Ga_{0.6}$As QCLs due to postgrowth heat treatment. Recently, we intentionally introduced graded interfaces by post-growth thermal annealing and examined its influence on the transport and optical properties of GaAs/(Al,Ga)As THz QCLs.[14] In Refs. 12 and 14, the Al composition grading was assumed to be a linear function of position approximated by a staircase with a certain number of steps. In order to keep the total amount of Al unchanged, the maximum Al content of the thin barriers was reduced.

Recently, Luna *et al.*[15,16] have discussed a more realistic model for the composition profile across semiconductor heterointerfaces based on experimental observations. Processes governing the interface formation appear to be more complex than a mere diffusion governed by Fick's law. In particular, cooperative binding of the atomic species during growth plays a key role in the interface formation.[17] The strong cooperative interactions result in two-dimensional island formation and lead to a sigmoidal distribution profile of the composition in the transition region between the two materials.[17]

In this Letter, we propose an efficient method for heterostructures with sigmoidal transition regions between the quantum well and barrier materials to solve the Schrödinger equation based on a plane-wave approximation with an error function approximating the interface profile. This method is beneficial for easy incorporation and fast computation.

As shown in Refs. 15–19, concentration profiles across semiconductor heterointerfaces are excellently reproduced by a function of the form

$$x(z) = \frac{x_0}{1 + e^{-\frac{z}{L_i}}}, \tag{1}$$

where x_0 denotes the nominal composition of one of the species, e.g., the Al composition in GaAs/(Al,Ga)As heterostructures, L_i is the interface parameter proportional to the width of the heterointerface, and z is the position across the interface along the growth direction. According to Ref. 15,

the interface width $W \approx 4.4\, L_i$. Figure 1(a) shows a simulated concentration profile across the interface between two binary compounds BC and AC described by the sigmoidal function according to Eq. (1). The use of a generalized sigmoidal expression gives a reliable and systematic quantification of the chemical interface through the interface parameter L_i. The sigmoidal function is the result of the prevalence of two-dimensional island growth as the mechanism governing the interface development.[17] Equation (1) agrees remarkably well with experimental composition profiles at the interface, even after post-growth thermal annealing.[15,18,19] Figure 1(b) displays a representative example of the experimental composition profile across an as-grown GaAs/(Al,Ga)As heterointerface obtained using transmission electron microscopy techniques[20] together with a fit using the sigmoidal function according to Eq. (1) with $L_i = 1.6$ MLs. The sample is prepared from the central part of the wafer. For comparison, the fit using an error function is also given in Fig. 1(b). Both curves (i.e., the sigmoidal and the error function) show almost the same behavior and provide a good description of the experimental data. The oscillating Al content at the plateau value (~30%) is due to the substrate rotation during growth and is not relevant for the present discussion on the interface grading. In the region of strongly changing slope at the positions of 5 MLs [cf. inset of Fig. 1(b)] and −5 MLs, the sigmoidal function [dashed line in Fig. 1(b)] allows for an improved fit to the experimental data. The reason is that Eq. (1) is the solution of the differential equation that describes the complex processes during growth beyond diffusion.[17] However, for an evaluation of the impact of interface grading on the transport and optical properties of heterostructures, Fig. 1(b) demonstrates that the sigmoidal function can be well approximated by the error function. For GaAs/(Al,Ga)As heterostructures, 1 and 4 MLs are reasonable lower and upper limits for the interface parameter L_i of as-grown samples, which may depend on the growth conditions. For example, Fujiwara *et al.*[11] showed well width fluctuations due to island growth of about 3 MLs in a GaAs/AlAs single QW. Post-growth thermal treatment may lead to larger values such as 8 MLs or even larger.[14]

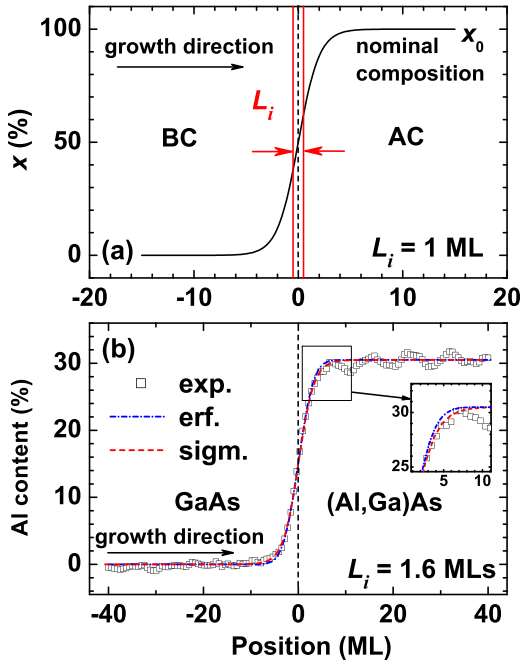

FIG. 1. (a) Simulated concentration profile across the interface between two binary compounds BC and AC described by a sigmoidal function. The arrows indicate the interface parameter L_i according to Eq. (1). (b) Experimental composition profile (squares) and sigmoidal function fit (dashed line) across an interface of GaAs/(Al,Ga)As. The fit using the error function (dashed-dotted line) is also given for comparison.

The nominal, i.e., step-like, potential profile is determined from the nominal compositions of the layers using the well-known expression including band gap bowing effects. However, for the shape of the interface grading, a linear dependence of the potential on the composition grading is a very good approximation. Thus, we can directly derive the error function potential profile from the nominal step-like profile. The step-like potential profile $V(z)$ can easily be converted into an error function shape $V_c(z)$ by convoluting the profile with a Gaussian function. We have

$$V_c(z) = \frac{1}{\sqrt{2\pi}\sigma}\int_{-\infty}^{+\infty} V(z_0) e^{-\frac{(z-z_0)^2}{2\sigma^2}} dz_0, \tag{2}$$

where σ denotes the standard deviation and is correlated with L_i. For a single interface at $z_0 = z_i$

$$V(z_0) = \begin{cases} 0 & \text{if } z_0 < z_i \\ V_0 & \text{if } z_0 \geq z_i, \end{cases} \tag{3}$$

where V_0 denotes the constant potential. We obtain

$$\begin{aligned} V_c(z) &= \frac{1}{2} V_0 \left[\operatorname{erf}\left(\frac{z - z_i}{\sqrt{2}\sigma} \right) + 1 \right] \\ &\approx \frac{1}{2} V_0 \left[\tanh\left(\sqrt{\frac{2}{\pi}} \frac{z - z_i}{\sigma} \right) + 1 \right] \\ &= \frac{V_0}{1 + e^{-\sqrt{\frac{2}{\pi}} \frac{2(z-z_i)}{\sigma}}}, \end{aligned} \tag{4}$$

where $\operatorname{erf}(y) \left[= \frac{2}{\sqrt{\pi}} \int_0^y e^{-t^2} dt \right]$ denotes the error function. By identifying $L_i = \sqrt{\frac{\pi}{2}} \frac{\sigma}{2}$ and $z_i = 0$, the last expression of Eq. (4) has the identical mathematical form as Eq. (1) demonstrating again that the error function is a good approximation of the sigmoidal function. For a potential with N barriers and considering two interfaces for each barrier, we obtain

$$\begin{aligned} V_c(z) &= \frac{V_0}{2} \sum_{q=1}^{N} \left[\operatorname{erf}\left(\frac{z - z_q}{\sqrt{2}\sigma_q} \right) - \operatorname{erf}\left(\frac{z - z_q - d_q}{\sqrt{2}\sigma_q} \right) \right] \\ &\approx \frac{V_0}{2} \sum_{q=1}^{N} \left[\tanh\left(\frac{z - z_q}{2L_i^q} \right) - \tanh\left(\frac{z - z_q - d_q}{2L_i^q} \right) \right], \end{aligned} \tag{5}$$

where d_q denotes the thickness, L_i^q is the interface parameter, and z_q is the left boundary of the q-th barrier.

For the two-band system, which is equivalent to an effective mass linearly dependent on energy, the Schrödinger equation can be written as[21]

$$\begin{pmatrix} V_s(z) & \frac{i\hbar}{\sqrt{2m_e\gamma(z)}}\frac{\partial}{\partial z} \\ \frac{i\hbar}{\sqrt{2m_e\gamma(z)}}\frac{\partial}{\partial z} & -\frac{\mu_0(z)}{\gamma(z)}+V_s(z) \end{pmatrix} \begin{pmatrix} \psi_1(z) \\ \psi_2(z) \end{pmatrix} = E \begin{pmatrix} \psi_1(z) \\ \psi_2(z) \end{pmatrix}, \tag{6}$$

where V_s denotes the function describing the edge of the conduction band, m_e is the free electron mass, γ is the nonparabolicity parameter in units of m_e per eV, and μ_0 is the band edge effective mass.

In the plane-wave approximation, we expand the envelope function $|\psi_n\rangle = \sum_j c_j^n \beta_j$, where $\beta_j = e^{ik_j z}/\sqrt{L}$ denotes an orthonormal basis, $k_j (= 2\pi j/L)$ is the wavenumber, and L is the period of the entire structure along the z-axis. Then, we obtain

$$\sum_{n,j} H_{n,j}^{m,\ell} c_j^n = E\, c_\ell^m, \tag{7}$$

where $H_{n,j}^{m,\ell} = \langle \beta_\ell | H_{mn} | \beta_j \rangle$ and $m(n) = 1$ or 2. Equation (7) is a set of coupled equations, which can be solved numerically after obtaining all $H_{n,j}^{m,\ell}$. The matrix elements $H_{1,j}^{1,\ell}$ are given by

$$H_{1,j}^{1,\ell} = \frac{1}{L}\int_0^L e^{-ik_\ell z}\, V(z)\, e^{ik_j z}\, dz. \tag{8}$$

In a similar way, we can obtain the components $H_{1,j}^{2,\ell}$, $H_{2,j}^{1,\ell}$ and $H_{2,j}^{2,\ell}$. For a step-like potential, $H_{1,j}^{1,\ell}$ is expressed as

$$H_{1,j}^{1,\ell} = \begin{cases} \frac{1}{L}\sum_{p=1}^{P}(V_p \Delta_p) & \text{if } j = \ell \\ \frac{1}{2\pi i(j-\ell)}\sum_{p=1}^{P}\left(V_p \Upsilon_{j\ell}\right) & \text{if } j \neq \ell, \end{cases} \tag{9}$$

with

$$\Upsilon_{j\ell} = e^{2\pi i \frac{j-\ell}{L}(z_p+\Delta_p)} - e^{2\pi i \frac{j-\ell}{L} z_p}, \tag{10}$$

where V_p denotes the constant potential, Δ_p is the thickness, z_p is the left boundary of the p-th layer, and P is the total number of layers. In general, $H_{1,j}^{1,\ell}$ may include the contributions from a step-like potential, an applied electrical field, doping, and the electron distributions, but for clarity we only discuss the result for a step-like potential.

For the incorporation of the interface grading, we use Eq. (2) in Eq. (8) and obtain the corresponding matrix elements, e.g., $H_{1,j}^{1,\ell}$

$$H_{1,j}^{1,\ell} = \begin{cases} \frac{1}{L}\sum_{p=1}^{P}(V_p \Delta_p) & \text{if } j = \ell \\ \frac{1}{2\pi i(j-\ell)}\sum_{p=1}^{P}\left(V_p \Upsilon_{j\ell}\right)\Phi_{j\ell} & \text{if } j \neq \ell, \end{cases} \tag{11}$$

where

$$\Phi_{j\ell} = e^{-\frac{(k_j-k_\ell)^2\sigma^2}{2}} = e^{-\frac{2\pi^2(j-\ell)^2\sigma^2}{L^2}} = e^{-16\pi\frac{(j-\ell)^2 L_i^2}{L^2}}. \tag{12}$$

This result shows that the incorporation of interface grading into the calculation results for the potential, effective mass, and nonparabolicity parameter in a simple multiplication of all Fourier components with the factor $\Phi_{j\ell}$, which allows for an efficient calculation of the transport and optical properties of complex structures. $\Phi_{j\ell}$ becomes 1 for $j = \ell$ ($k_j - k_\ell = 0$, zero component), while $\Phi_{j\ell}$ decreases with the increase of $j - \ell$ or $k_j - k_\ell$. Thus, the high-frequency components (large values of $k_j - k_\ell$) lead to small values of $\Phi_{j\ell}$ and a reduction of $H_{1,j}^{1,\ell}$. At the same time, the average Al composition is automatically kept constant for all values of L_i due to the convolution with the Gaussian function. The interface grading is simply defined by the value of L_i, which is also convenient for the practical use of the model, if we can assume the same value for L_i for all the layers of the structure.

As a simple example, we examine the influence of L_i on the energy separation E_{sp} in a single QW. Figure 2 gives the conduction band profile and the lowest two subbands of a GaAs/$Al_{0.25}Ga_{0.75}As$ single QW at a field strength of $F = 3$ kV/cm for three values of L_i (1, 4, and 8 MLs). Obviously, the interface parameter L_i has an impact on the energy separation between the two subbands E_{sp}. For $L_i = 0$ and $L_i = 1$ ML, the values of E_{sp} are similar, namely, 84.3 meV and 85.9 meV, respectively. When L_i increases from 1 to 4 MLs, E_{sp} increases from 85.9 to 92.3 meV, which corresponds to a blue shift. When L_i increases from 4 to 8 MLs, E_{sp} decreases from 92.3 to 73.5 meV, which corresponds to a redshift. Even for this simple system, the influence of interface grading on the separation of the energy levels has to be taken into account. This behavior is similar to that of coupled Si/SiGe QWs discussed in Ref. 4.

An additional important feature in semiconductor heterostructures, in particular also in QCL structures, is the resonant coupling between subbands in adjacent QWs, where the field strength for the resonant coupling (F_r) depends on the potential profile. As a second example, we thus check the influence of the interface grading on the resonant coupling in a double QW. Figure 3 shows the subband structure of a GaAs/$Al_{0.25}Ga_{0.75}As$ double QW at F_r for $L_i = 1$ and 4 MLs. The resonant field strength F_r is 5.2 kV/cm for $L_i = 0$

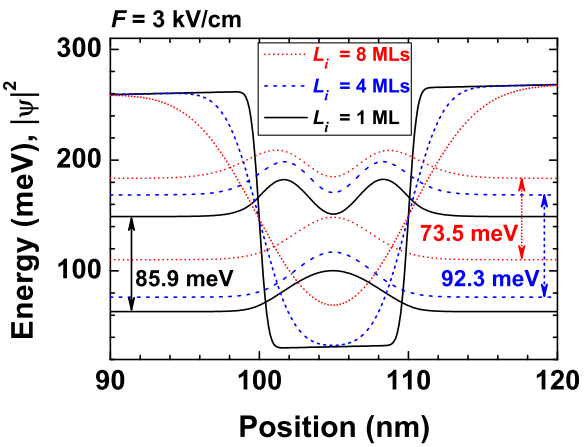

FIG. 2. Conduction band profile and lowest two subbands of a GaAs/$Al_{0.25}Ga_{0.75}As$ single QW at a field strength of 3 kV/cm for different L_i. The thickness of the GaAs QW is 10 nm. The arrows indicate the transition energy E_{sp} between the two subbands. For $L_i = 0$, E_{sp} is 84.3 meV (not shown here).

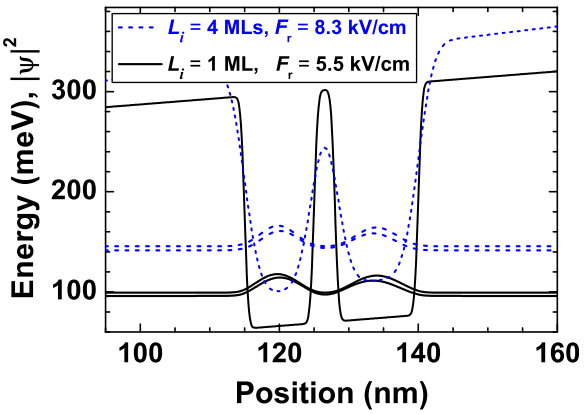

FIG. 3. Conduction band profile and lowest two subbands of a GaAs/$Al_{0.25}Ga_{0.75}As$ double QW at the resonant field strength F_r for $L_i = 1$ and 4 MLs. The thicknesses of the QWs are 10 nm and 12 nm, separated by a 3-nm-thick $Al_{0.25}Ga_{0.75}As$ barrier. For $L_i = 0$, the resonant field strength is 5.2 kV/cm (not shown here).

(not shown), 5.5 kV/cm for $L_i = 1$ ML, and 8.3 kV/cm for $L_i = 4$ MLs. Furthermore, the energy level at the resonant field strength is higher for the larger interface parameter ($L_i = 4$ MLs), similar to the case of a single QW. Obviously, the interface grading may have a significant effect on the resonant coupling and should be taken into consideration for the evaluation of the transport properties of heterostructures.

Finally, we exemplarily show the effect of interface grading on the properties of a QCL structure. Figures 4(a) and 4(b) depict the subband structure of the QCL design B1 in Ref. 22 for $L_i = 1$ and 4 MLs, respectively. For

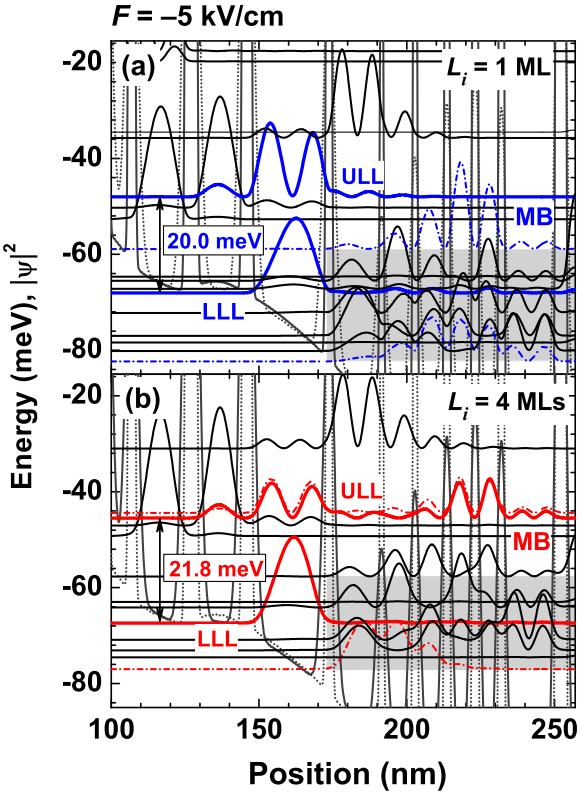

FIG. 4. Conduction band profile and lowest subbands for the QCL design B1 in Ref. 22 at a field strength of −5 kV/cm for (a) $L_i = 1$ and (b) 4 MLs. The solid arrows indicate the transitions between the ULL and LLL. The transition energy for $L_i = 0$ is 20.0 meV (not shown here).

comparison, the band profile of $L_i = 4$ MLs is given as a dashed line in Fig. 4(a), while that of $L_i = 1$ ML is indicated by the dashed line in Fig. 4(b). The energy difference between the upper laser level (ULL) and the lower laser level (LLL) in Fig. 4 corresponds to the energy of the laser emission. We find that, similar to the single QW structure (cf. Fig. 2), E_{sp} increases with increasing L_i. For $L_i = 0$ (not shown), 1 ML and 4 MLs, $E_{sp} = 20.0$ meV (4.84 THz), 20.0 meV (4.84 THz), and 21.8 meV (5.27 THz), respectively. The result is a blue shift of the lasing frequency of 9.0%. At the same time, the interface grading has a notable impact on the formation of the minibands (MBs) such as the energy positions and shape of some wavefunctions within the MBs (dashed-dotted lines in Fig. 4). Since the electron transport in the structure is facilitated by MB formation, the modification of the MBs due to grading can directly influence the transport properties of the structure. Therefore, the effect of interface grading on MB formation should also be taken into consideration for the design of complex heterostructures.

In summary, we have proposed an efficient model for the incorporation of interface grading into the calculations of the transport and optical properties of semiconductor heterostructures. The model takes into account the realistic interface profile by approximating the sigmoidal function through an error function. In the plane-wave approximation, this approximation does not result in a significant increase of the computation time. This improved model allows for an efficient evaluation of the influence of interface grading on intersubband transition energies, field strength for the resonant coupling of subbands in adjacent quantum wells, and miniband formation. By applying this model, we expect a significant improvement for the design of complex heterostructures.

The authors would like to thank O. Marquardt for helpful discussions as well as R. Hey and M. Höricke for sample growth. We also acknowledge partial financial support by the Deutsche Forschungsgemeinschaft.

[1]E. H. Li, B. L. Weiss, and K.-S. Chan, IEEE J. Quantum Electron. **32**, 1399 (1996).
[2]V. Gavryushin, Cent. Eur. J. Phys. **10**, 459 (2012).
[3]A. Valavanis, Z. Ikonić, and R. W. Kelsall, Phys. Rev. B **77**, 075312 (2008).
[4]A. Valavanis, Z. Ikonić, and R. W. Kelsall, J. Opt. A: Pure Appl. Opt. **11**, 054012 (2009).
[5]T. Unuma, M. Yoshita, T. Noda, H. Sakaki, and H. Akiyama, J. Appl. Phys. **93**, 1586 (2003).
[6]Y. V. Flores, S. S. Kurlov, M. Elagin, M. P. Semtsiv, and W. T. Masselink, Appl. Phys. Lett. **103**, 161102 (2013).
[7]C. Deutsch, H. Detz, T. Zederbauer, A. M. Andrews, P. Klang, T. Kubis, G. Klimeck, M. E. Schuster, W. Schrenk, G. Strasser, and K. Unterrainer, Opt. Express **21**, 7209 (2013).
[8]C. W. I. Chang, Q. Hu, and J. L. Reno, Appl. Phys. Lett. **103**, 151117 (2013).
[9]S. Yuan, Y. Kim, H. H. Tan, C. Jagadish, P. T. Burke, L. V. Dao, M. Gal, M. C. Y. Chan, E. H. Li, J. Zou, D. Q. Cai, D. J. H. Cockayne, and R. M. Cohen, J. Appl. Phys. **83**, 1305 (1998).
[10]K. Fujiwara, K. Kanamoto, N. Tsukada, H. Miyatake, and H. Koyama, J. Appl. Phys. **66**, 1488 (1989).
[11]K. Fujiwara, K. Kanamoto, and N. Tsukada, Phys. Rev. B **40**, 9698 (1989).
[12]J. S. Roberts, R. P. Green, L. R. Wilson, E. A. Zibik, D. G. Revin, J. W. Cockburn, and R. J. Airey, Appl. Phys. Lett. **82**, 4221 (2003).

[13]S. Anders, W. Schrenk, T. Roch, C. Pflügl, and G. Strasser, Appl. Phys. Lett. **84**, 164 (2004).
[14]R. Sharma, L. Schrottke, M. Wienold, K. Biermann, A. Tahraoui, and H. T. Grahn, J. Phys. D: Appl. Phys. **46**, 305107 (2013).
[15]E. Luna, F. Ishikawa, P. D. Batista, and A. Trampert, Appl. Phys. Lett. **92**, 141913 (2008).
[16]E. Luna, B. Satpati, J. B. Rodriguez, A. N. Baranov, E. Tournié, and A. Trampert, Appl. Phys. Lett. **96**, 021904 (2010).
[17]E. Luna, Á. Guzmán, A. Trampert, and G. Álvarez, Phys. Rev. Lett. **109**, 126101 (2012).
[18]O. Hulko, D. A. Thompson, and J. G. Simmons, IEEE J. Sel. Top. Quantum Electron. **14**, 1104 (2008).
[19]O. Hulko, D. A. Thompson, B. J. Robinson, and J. G. Simmons, J. Appl. Phys. **105**, 073507 (2009).
[20]E. G. Bithell and W. M. Stobbs, Philos. Mag. A **60**, 39 (1989).
[21]L. Schrottke, M. Giehler, M. Wienold, R. Hey, and H. T. Grahn, Semicond. Sci. Technol. **25**, 045025 (2010).
[22]L. Schrottke, M. Wienold, R. Sharma, X. Lü, K. Biermann, R. Hey, A. Tahraoui, H. Richter, H.-W. Hübers, and H. T. Grahn, Semicond. Sci. Technol. **28**, 035011 (2013).